The Cryosphere Discuss., https://doi.org/10.5194/tc-2018-38
Manuscript under review for journal The Cryosphere
Discussion started: 29 March 2018

The Cryosphere Discussions
Open Access
EGU

Can ice-cliffs explain the "debris-cover anomaly"? New insights from Changri Nup Glacier, Nepal, Central Himalaya

Fanny Brun[1,2], Patrick Wagnon[1,3], Etienne Berthier[2], Joseph M. Shea[3,4,5], Walter W. Immerzeel[6], Philip D.A. Kraaijenbrink[6], Christian Vincent[1], Camille Reverchon[1], Dibas Shresta[7], and Yves Arnaud[1]

[1]Univ. Grenoble Alpes, CNRS, IRD, Grenoble INP, IGE, F-38000 Grenoble, France
[2]LEGOS, Université de Toulouse, CNES, CNRS, IRD, UPS, F-31400 Toulouse, France
[3]International Center for Integrated Mountain Development, Kathmandu, Nepal
[4]Center for Hydrology, University of Saskatchewan, Saskatoon, Canada
[5]Geography Program, University of Northern British Columbia, Prince George, Canada
[6]Department of Physical Geography, Faculty of Geosciences, Utrecht University, Utrecht, the Netherlands
[7]Central Department of Hydrology and Meteorology, Tribhuvan University, Kathmandu, Nepal

Correspondence: Fanny Brun (fanny.brun@univ-grenoble-alpes.fr)

Abstract. Ice cliff backwasting on debris-covered glaciers is recognized as an important process, potentially responsible for the so-called "debris-cover anomaly", i.e. the fact that debris-covered and debris-free glacier tongues appear to have similar thinning rates in Himalaya. In this study, we assess the total contribution of ice cliff backwasting to the net ablation of the tongue of the Changri Nup Glacier over two years. Detailed terrestrial photogrammetry surveys were conducted on select ice cliffs in November 2015 and 2016, and the entire glacier tongue was surveyed with unmanned air vehicles (UAVs) and Pléiades tri-stereo imagery in November 2015, November 2016, and November 2017. The total difference between the volume loss from ice cliffs measured with the terrestrial photogrammetry, considered as the reference data, and the UAV and Pléiades was less than 3 % and 7 %, respectively, demonstrating the ability of these datasets to measure volume loss from ice cliffs. For the period November 2015–November 2016 (resp. November 2016–November 2017), using UAV and Pléiades over the entire glacier tongue, we found that ice cliffs, which cover 7 % (resp. 8 %) of the planar area, contribute to 23 $\pm$ 5 % (resp. 24 $\pm$ 5 %) of the total net ablation of Changri Nup Glacier tongue. Ice cliffs have a net ablation rate 3.1 $\pm$ 0.6 (resp. 3.0 $\pm$ 0.6) times higher than the average glacier tongue surface. However, on Changri Nup Glacier, ice cliffs cannot compensate for the reduction of ablation due to debris-cover. Reduced ablation and lower emergence velocities on debris-covered glacier tongues could be responsible for the debris-cover anomaly.

1 Introduction

Ablation areas in High Mountain Asia (HMA) are heavily debris-covered, meaning that a potentially large part of melt water originates from ice ablation of debris-covered glacier tongues (Kraaijenbrink et al., 2017). Numerous studies have demonstrated that a debris layer thicker than 5–10 cm has a dominant insulating effect and dampens the ablation of ice beneath it (e.g., Østrem, 1959; Nicholson and Benn, 2006; Reid and Brock, 2010; Reznichenko et al., 2010; Lejeune et al., 2013). Yet counter-intuitively, similar thinning rates (change in glacier surface elevation over time) were observed for clean ice and debris-covered

The Cryosphere Discuss., https://doi.org/10.5194/tc-2018-38
Manuscript under review for journal The Cryosphere
Discussion started: 29 March 2018

ice at similar elevations across HMA (Gardelle et al., 2013; Kääb et al., 2012), in the Khumbu region (Nuimura et al., 2012), the Langtang catchment (Pellicciotti et al., 2015), the Kangri Karpo Mountains (Wu et al., 2018), for the Kanchenjunga Glacier (Lamsal et al., 2017) and the Siachen Glacier (Agarwal et al., 2017). This has been referred to as the "debris-cover anomaly" (Pellicciotti et al., 2015).

Two main hypotheses have been proposed to explain this anomaly. First, debris-covered tongues have a lower emergence velocity compared with debris-free tongues (Anderson and Anderson, 2016; Banerjee, 2017). As a result, even though debris-covered tongues have less negative surface mass balance compared to clean ice glaciers, their thinning rates (surface mass balance rate minus emergence velocity) are similar. Alternatively, while ablation rates are reduced by thick debris, supra-glacial features such as ice cliffs and ponds could be "hot spots" of ablation and thus contribute disproportionally to the tongue-averaged ablation (Sakai et al., 1998, 2002; Reid and Brock, 2014; Immerzeel et al., 2014; Pellicciotti et al., 2015; Steiner et al., 2015; Miles et al., 2016; Buri et al., 2016a).

In order to test the second hypothesis, there is a need to calculate the total contribution of ice cliffs to the tongue-wide surface mass balance. For simplicity, hereafter we abusively use the term net ablation instead of surface mass balance as we focus only on the ablation areas. We introduce a variable, noted hereafter p, to quantify the enhanced ablation at ice cliffs. The variable p, defined as the spatially integrated ratio between the cliff net ablation and the glacier tongue net ablation, is used to quantify enhanced ablation due to ice cliffs:

$$p = \frac{\dot{b}_C}{\dot{b}_T} = \frac{\Delta V_C}{A_C} \times \frac{A_T}{\Delta V_T} \tag{1}$$

where $\dot{b}$ is the net ablation, ΔV is the volume loss and A is the area, in each case the subscript refers to the cliff (C) or the glacier tongue (T).

Most previous attempts to estimate the value of p were based on modelling and found values to be between 5 to 7 (Juen et al., 2014; Reid and Brock, 2014), around 14 (Buri et al., 2016b) or even more than 35 (Sakai et al., 1998). Two studies have quantified p using direct observations: Brun et al. (2016) found $p = 6$ over Lirung Glacier by extrapolating volume losses measured on a limited number of cliffs and Thompson et al. (2016) found a value of 8 by digital elevation model (DEM) differencing at Ngozumpa Glacier in the Nepalese Himalaya.

The emergence velocity (w_e) of ice for debris-covered glaciers has been found to be significantly different from zero for some cases, but it has typically been neglected in the calculation of p. Values of w_e equal to 5.7–6.4 $\pm$ 3.9 m a^{-1} (Nuimura et al., 2011), 0.41 $\pm$ 0.05 m a^{-1} (Vincent et al., 2016) and 0.00–0.35 $\pm$ 0.10 m a^{-1} (Nuimura et al., 2017) have been found for, respectively, the debris-covered tongues of Khumbu, Changri Nup and Lirung glaciers in Nepal. Emergence velocities will affect the thinning rates of debris-covered ice and ice cliffs equally. But since the cliffs ablate at higher rate, their thinning rate is relatively less influenced than the thinning rate of debris-covered ice. As a consequence, the ratio of the cliff thinning rate divided by the mean tongue thinning rate will overestimate p. To correctly estimate p and the fraction of total ice cliff net ablation, it is therefore needed to correct the thinning rates with the emergence velocity in order to calculate net ablation rates.

Recent studies advocate the use of terrestrial photogrammetry to understand patterns of ice cliff retreat (e.g., Watson et al., 2017). Nevertheless, these data can only be collected in the field with some difficulty, and can only be acquired on a limited

number of cliffs. Remote sensing platforms (unmanned air vehicles [UAVs], satellites) offer the potential to provide high resolution topographic data with a glacier-wide or region-wide coverage but have not yet been evaluated for detailed multi-temporal monitoring of ice cliffs. Here we test the possibility to use gridded elevation data (i.e. DEMs) obtained from both UAV and Pléiades imagery to assess the total ice cliff contribution to the tongue-wide net ablation.

In this study, we use three very high resolution topographic datasets based on terrestrial photogrammetry, UAV imagery, and Pléiades imagery collected over the tongue of Changri Nup Glacier, Nepal between 2015 and 2017. From the terrestrial photogrammetry, 3D models of 12 cliffs are created to calculate reference ice cliff volume losses (2015 to 2016). We introduce a new method based on DEM differencing, which takes into account geometric changes induced by glacier flow and apply it to the UAV and Pléiades imagery. The new method is validated with the terrestrial photogrammetric estimates and applied to the entire Changri Nup Glacier tongue in order to evaluate the fraction of the tongue-wide net ablation due to ice cliffs.

2 Study area

This study focuses on the debris-covered part of the tongue of the Changri Nup Glacier, Everest region, Nepal (Fig. 1). We use the same glacier tongue outline as Vincent et al. (2016), which was derived from a combination of UAV imagery, field measured velocity fields and field expertise. It is different from the outline available in the Randolph Glacier Inventory 6.0 (Pfeffer et al., 2014), which includes the nearby West Changri Nup Glacier in the same outline (Sherpa et al., 2017). The debris-covered part of the tongue has an area of 1.49 ± 0.16 km^2 (Fig. 1). We focus first on 12 ice cliffs that were ground surveyed (Table 1 and Fig. 1), before extending the analysis to more than 140 ice cliffs of various sizes (Fig. 1). The planar area of these cliffs were $69\,876 \pm 14\,000$ m^2, $71\,826 \pm 14\,000$ m^2 and $69\,537 \pm 14\,000$ m^2 in November 2015, in November 2016 and in November 2017, respectively (see section 4.4.4 for the uncertainty assessment for the cliff planar area).

3 Data

3.1 Terrestrial photogrammetry

We collected terrestrial photographs during two field campaigns: 24–28 November 2015 and 9–12 November 2016. We surveyed a total of 12 cliffs (Table 1) with methods similar to Brun et al. (2016) and Watson et al. (2017). Between 200 and 400 photographs of each cliff were taken from various camera positions using a Canon EOS5D Mark II digital reflex camera with a Canon 50 mm f/2.8 fixed focal length lens (Vincent et al., 2016). For each cliff, we derive point clouds (PCs) and triangulated irregular networks (TINs) with Agisoft Photoscan 1.3.4 professional edition (Agisoft, 2017). In order to align the photographs and georeference the final point clouds and derived products, between 7 and 17 ground control points (GCPs) made of pink fabric were spread around each cliff. GCPs positions were surveyed with a Topcon differential global positioning system (DGPS) unit with a precision of $\sim$10 cm. All markers were used as GCPs and therefore no independent markers were available for validation. After optimization of the photographs alignment, the marker residuals were on average 27 cm for the

2015 campaign and 18 cm for the 2016 campaign. The 3D area of the surveyed cliffs ranged from 600 m^2 to more than 11 000 m^2 (Table 1).

3.2 UAV photogrammetry

UAV imagery of Changri Nup Glacier was obtained in November 2015, November 2016, and November 2017 using the fixed-wing eBee UAV manufactured by senseFly (Table 2). In 2015, five separate flights with the eBee were performed to cover the surface of the glacier over the course of 3 days, i.e. 22–24 November. The imagery was processed into a dense point cloud using the Structure from Motion (SfM) algorithm (Agisoft, 2017), which was subsequently used to produce a 10 cm resolution orthomosaic and a 20 cm DEM. The data was georeferenced using a set of 24 GCPs that were well spatially distributed and measured using the Topcon DGPS (Fig. S1). Based on 10 additional independent GCPs, the error of the UAV products was measured independently and determined to be 4 cm horizontal and 10 cm vertical, which is in the range of expected accuracy (Gindraux et al., 2017). For a detailed description of the data processing refer to Vincent et al. (2016) and Kraaijenbrink et al. (2016a).

On 10 November 2016 we surveyed Changri Nup in three successful flights with the eBee UAV. In the three flights the eBee captured a total of 475 images using the mounted Sony Cyber-shot WX DSC-WX220. The SfM procedure that we implemented in Agisoft Photoscan Professional version 1.2.6 to process the imagery is equal to the procedure that we used for the 2015 data (Vincent et al., 2016; Kraaijenbrink et al., 2016a) to enable an optimal comparison. Also for this dataset, an orthomosaic and a gridded DEM were produced from the generated dense point cloud with 10 cm and 20 cm resolution, respectively. To georeference the 2016 UAV imagery, we distributed a total of 17 markers on the glacier and measured their coordinates with the Topcon DGPS. Unfortunately, due to time constraints, the resulting spatial distribution of the markers was suboptimal (Fig. S1). Using only these markers as GCPs had considerable consequences for processing accuracy, and we therefore defined 16 additional virtual tie points for which we sampled the coordinates from the November 2015 UAV orthomosaic and DEM (Fig. S1). For the tie points, we selected specific features on boulders that were clearly identifiable on both the 2015 and 2016 image sets. The use of virtual tie points requires stable terrain (Immerzeel et al., 2014), i.e. the coordinates of the features should not change over time. We have therefore only selected points in stable areas in the vicinity of the glacier, which we determined from visual inspection of the Pléiades orthoimages and DEMs.

In 2017, we performed the same measurements as in 2015 in three separate flights on 23 November, using 30 GCPs (Fig. S1). The residuals, based on 6 independent check points were 10 cm in horizontal and 14 cm in vertical .

3.3 Pléiades tri-stereo photogrammetry

Three triplets of Pléiades images were acquired over the study area on 22 November 2015, on 13 November 2016 and on 24 October 2017 (Table 3). The along track angles of the acquisitions gave base to height ratios ensuring suitable stereo capabilities (e.g., Belart et al., 2017). For each acquisition, we derived a 2 m resolution DEM and a 0.5 m resolution orthoimage using the Ames Stereo Pipeline (ASP; Shean et al., 2016) using only the rational polynomial coefficients (RPCs) provided with the imagery (no GCP) and the same processing parameters as Marti et al. (2016). We used the *stereo* routine of ASP to derive one

PC from each triplet of images, which was gridded into a single 2 m DEM using the *point2dem* routine. The orthoimages were generated from the image closest to the nadir using the *mapproject* function and a 2 m resolution DEM, which was gap-filled with 4 and 8 m DEM resolutions derived similarly. This ensured to obtain sharp and gap-free images.

Each Pléiades orthoimage was co-registered to the corresponding UAV orthomosaic, by matching boulders on stable ground visually. We check the accuracy of this co-registration by calculating the median displacement on a 2.4 km^2 stable area off-glacier. An east to west residual displacement of 0.05 m and a north to south residual displacement of -0.09 m was identified after co-registration. This absolute co-registration was needed to compare the UAV and Pléiades datasets, but would not be necessary while working with Pléiades data only. In the latter case, the robustness of the Pléiades processing based on RPCs only would be sufficient to co-register the images and DEMs relatively using automatic co-registration methods. Each Pléiades DEM was shifted with the same horizontal displacement as the corresponding orthoimage (Table 3). Automatic co-registration methods applied to the manually-shifted DEMs (Berthier et al., 2007; Nuth and Kääb, 2011) resulted in no improvement of the standard deviation of elevation changes on stable terrain. Thus, no further horizontal shift was applied. The vertical shift between the two Pléiades DEMs was calculated as the median elevation change on stable terrain and was equal to -7.43 m and -3.31 m for the periods November 2015–November 2016 and November 2016–November 2017, respectively. We corrected this vertical median bias by subtracting this value to the elevation difference map. We tested the dependency of the elevation changes over stable terrain to the slope, aspect and curvature and found no dependency to these parameters (Fig. S2).

For these three datasets, the duration between acquisition dates were 350 to 381 days. All displacements and volumes have been linearly adjusted (divided by the number of days between the acquisition dates and the total number of days in a year) to obtain annual velocities and change rates.

3.4 Update of existing datasets

3.4.1 Surface velocity fields

Surface velocity fields were derived from the correlation of the Pléiades orthoimages and UAV orthomosaics using COSI-corr (Leprince et al., 2007). The UAV orthomosaics were resampled to a resolution of 0.5 m to match one of the Pléiades orthoimages. For both data sets we choose an initial correlation window size of 256 pixels and a final size of 16 pixels (Kraaijenbrink et al., 2016a). The step was set to 16 pixels, leading to a final grid spacing of 8 m.

The raw correlation outputs were filtered to maintain pixels with a signal to noise ratio larger than 0.9. We manually removed pixels at ice cliff locations, as cliff retreat lead to large geometric changes and therefore poor correlation. These outputs were filtered with a 9×9 pixel window moving median filter and then gap-filled with a bilinear interpolation (Fig. 2). The patterns of displacement from UAV and Pléiades are in very good agreement. The velocities measured with Pléiades match well with the field data, with the notable exception of a stake located where the velocity gradient is high and for which the correlation between the Pléiades images could not work due to snow, leading to a poor bilinear interpolation (Fig. S3). Nevertheless, the

The Cryosphere Discuss., https://doi.org/10.5194/tc-2018-38
Manuscript under review for journal The Cryosphere
Discussion started: 29 March 2018

maximum displacement is lower in the remote sensing data (around 11 m a^{-1}), than the 2011–2015 field data (around 12 m a^{-1}; Vincent et al., 2016). This is due to a slowdown of the glacier observed in the 2015–2016 field data.

3.4.2 Emergence velocity

In order to evaluate the mean net ablation of the tongue from the rate of elevation change, we estimate the mean emergence velocity (w_e) for the period November 2015–November 2016 and for the period November 2016–November 2017 using the flux gate method of Vincent et al. (2016). This method requires an estimate of ice flux through a cross-section of the glacier, and is based here on measurements of ice depth and surface velocity along a profile upstream of the debris-covered tongue (Figs. 1 and 2). Between November 2015–November 2016 and November 2016–November 2017, the cross sectional area was reduced from 76 900 $\pm$ 100 m^2 to 76 340 $\pm$ 100 m^2, based on the 0.86 m a^{-1} thinning rate measured for the November 2015–November 2017 period along the profile. The glacier tongue area was considered unchanged at 1.49 $\pm$ 0.16 km^2. For the period November 2015–November 2016 (resp. November 2016–November 2017), the glacier slowed down compared with the 2011–2014 period and the centerline velocity was equal to 10.8 m a^{-1} (resp. 11.1 m a^{-1}), leading to an assumed mean surface velocity along the upstream profile of 8.1 $\pm$ 0.6 m a^{-1} (resp. 8.3 $\pm$ 0.6 m a^{-1}) and a depth-averaged velocity of 6.5 $\pm$ 0.6 m a^{-1} (resp. 6.6 $\pm$ 0.6 m a^{-1}) (Vincent et al., 2016). The incoming ice flux for the period was thus 499 700 $\pm$ 46 130 m^3 a^{-1} (resp. 503 840 $\pm$ 45 800 m^3 a^{-1}) corresponding to w_e = 0.33 $\pm$ 0.05 m a^{-1} (resp. 0.34 $\pm$ 0.05 m a^{-1}), when distributed over the ablation area. This emergence velocity is ~20 % lower than estimated for the 2011-2015 period (Vincent et al., 2016), due to both the thinning and deceleration of the glacier. As the difference in w_e between the two periods is insignificant, we consider w_e to be constant and equal to w_e = 0.33 $\pm$ 0.05 m a^{-1} for the rest of this study.

4 Methods

4.1 Point cloud deformation

Every point on the glacier surface moves with a horizontal velocity u_s, along a surface slope α and is advected upwards following the vertical velocity w_s (Fig. 3; Hooke, 2005; Cuffey and Paterson, 2010):

$$w_s = u_s \tan\alpha + w_e \quad (2)$$

When DEM differencing is applied, observed thinning rates at every point on the glacier surface is a combination of net ablation and displacement caused by glacier flow. In order to measure only the volume loss associated with the net ablation, we deformed the PCs of the datasets acquired in November 2015 and in November 2016 to account for three-dimensional glacier flow between November 2015 and November 2016 and between November 2016 and November 2017, respectively. For the terrestrial photogrammetry and UAV data, we applied these deformations directly to each point of the PCs. For the Pléiades data, we artificially oversampled the DEM on a 0.5 m resolution grid and converted this DEM to a PC, using the *gdal_translate*

function. All the points of the PCs were displaced in x, y and z direction:

$$\begin{cases} x_{t+dt} = x_t + u_{s,x}dt \\ y_{t+dt} = y_t + u_{s,y}dt \\ z_{t+dt} = z_t + w_s dt \end{cases} \quad (3)$$

where $u_{s,x}$ and $u_{s,y}$ are the x and y components of the horizontal velocity, dt is the duration between the two acquisitions and z is the glacier surface elevation.

Even though w_e is likely to be spatially variable, we consider it to be homogeneous over the whole ablation tongue. The horizontal velocity u_s was directly taken from the bilinear interpolation of the Pléiades velocity field (Fig. 2). The term $u_s \tan\alpha$, can be expressed as:

$$u_s \tan\alpha = \frac{z(x + u_{s,x}dt, y + u_{s,y}dt) - z(x,y)}{dt} \quad (4)$$

As the ice flows along the glacier mean slope instead of the rough local surface slope, we extracted z from a smoothed version of the Shuttle Radar Topography Mission (SRTM) DEM. In order to smooth the SRTM DEM, we filtered it with a Gaussian function using a 30 pixel kernel size to calculate $u_s \tan\alpha$ (Fig. S4).

For the Pléiades and UAV data, we then gridded the deformed PCs using the *point2dem* ASP function (Shean et al., 2016) and derived the associated maps of elevation changes (Figs. 4 and 5).

4.2 Ice cliff volume change from TINs

In order to measure the volume changes due to cliff retreat from the TINs derived from terrestrial photos, we applied the method from Brun et al. (2016) with some methodological improvements. First, the field of displacement was assumed to be homogenous at the cliff scale in Brun et al. (2016). In this study, we use interpolated values of the local field of displacement with a resolution of 8 m. This is an important methodological refinement for cliffs over fast flowing glaciers with a rotational component. Second, we added more analogous points in the cliff edge triangulation method. Analogous points are points that are assumed to match in the two acquisitions (e.g. the corners of cliffs). Brun et al. (2016) discretized the triangulation problem assuming that the final number of points was equal on the upper and on the lower side of the cliff outline (i.e. implicitly assuming that the two corners of the cliffs were the only analogous points). In this study, the operator can choose how many analogous points are needed to link the two cliff outlines. Consequently, the method is now able to handle larger geometry changes than previously, under the assumption that some analogous parts of the cliffs are identifiable on both cliff outlines.

4.3 Ice cliff volume change from DEMs

We measured the cliff volume change from DEMs simply as the mean elevation change corrected from glacier flow below a cliff mask multiplied by the projected planar area of the mask. The cliff mask was defined as the union of the shapefiles of the cliff outlines, and is called the cliff footprint and noted A_{2D} hereafter. The cliff outlines were manually delineated both on the Pléiades and UAV orthoimages for November 2015, November 2016 and November 2017. For each acquisition, we

The Cryosphere Discuss., https://doi.org/10.5194/tc-2018-38
Manuscript under review for journal The Cryosphere
Discussion started: 29 March 2018

used deformed outlines of November 2015 and November 2016 cliffs when working with the corresponding deformed DEM difference. We manually edited the cliff mask to make sure we included the terrain along which the cliff retreated. In particular, this implied linking the corners of the cliff outlines of the two acquisitions in many cases.

4.4 Sources of uncertainty

The main sources of uncertainties on the volume loss estimates are (1) the uncertainty on the spatial distribution of the vertical velocity (σ_e); (2) uncertainties of the horizontal surface displacement (σ_d); (3) uncertainty introduced by the displacement along the slope (σ_w); (4) uncertainties of the cliff outlines delineation (σ_m) and (5) uncertainties of the various representations of the glacier surface in TINs and DEMs (σ_z). The first, second and third sources of uncertainties are common to the three datasets and the third and fourth ones are specific to each dataset. We assume these five sources of uncertainty to be independent.

4.4.1 Emergence velocity

We calculated a mean emergence velocity for the tongue of 0.33 $\pm$ 0.05 m a^{-1}, but as the spatial variability was unknown extreme values of emergence velocities were tested to estimate σ_e. We choose 0.00 m a^{-1} as a lower limit because the emergence velocity is positive in the ablation area (Hooke, 2005; Cuffey and Paterson, 2010). The maximum net ablation measured with stakes within the period 2014–2016 on the tongue of Changri Nup was chosen as an upper limit equal to 2.22 m a^{-1} (Vincent et al., 2016). We tested these values on the terrestrial photogrammetry-based volume change estimate of each cliff (Fig. 6a). Except for cliff 11, the relative volume change that resulted from the test was always below +40 % for an increase in the emergence velocity and -5 % for a decrease in the emergence velocity. Cliff 11 likely exhibits a high sensitivity to the emergence velocity due to its relatively shallow slope and its very small volume loss (Table 1 and S1). The tested range of values of emergence velocities are rather extreme for the case of Changri Nup Glacier, and we therefore assumed that the uncertainty due to the emergence velocity was equal to the median of the relative volume change for an increase in the emergence velocity (23 %). As a consequence, $\sigma_e = 0.23V$, where V is the cliff volume change.

4.4.2 Horizontal displacement

The quality of the horizontal surface displacement derived from Pléiades orthoimages was evaluated by comparison with field measurements of the surface displacement. The median of the absolute difference between the 16 field measurements (stakes and marked rocks) and the corresponding Pléiades measurements was 30.8 cm. We therefore assumed that the uncertainty introduced by the horizontal displacement (σ_d) is 30 cm. The conversion into volumetric uncertainty, σ_d was made by multiplying this uncertainty by the cliff 3D area (A_{3D}) for the terrestrial photogrammetry and by the cliff footprint area (A_{2D}) for the UAV and Pléiades (Table 1).

The Cryosphere Discuss., https://doi.org/10.5194/tc-2018-38
Manuscript under review for journal The Cryosphere
Discussion started: 29 March 2018

4.4.3 Displacement along the glacier slope

The uncertainty on $u_s \tan\alpha$ depends mostly on the uncertainty on the mean slope of the surrounding glacierized surface (Hooke, 2005). We evaluated kernel sizes of 5 and 60 to filter the SRTM DEM and found respective mean elevation changes on the cliff mask of -0.51 and -0.33 m a^{-1}. As these values correspond to relatively sharp and very smooth DEMs, half of the difference between these two values (10 cm) is a good proxy for the uncertainty due to this correction. We converted this uncertainty into a volumetric uncertainty (σ_w) by multiplying it by the cliff 3D area (A_{3D}) for the terrestrial photogrammetry and by the cliff footprint area (A_{2D}) for the UAV and Pléiades.

4.4.4 Cliff mapping

The uncertainty on the cliff mapping from Pléiades orthoimages was empirically assessed by asking eight different operators (most of the co-authors of this study) to map six cliffs for which we had reference outlines from the terrestrial photogrammetry. The operators had access to the Pléiades orthoimage of November 2016 and to the corresponding slope map. We calculated a normalized length difference defined as the difference between the area mapped by the operator and the reference area divided by the outline perimeter. The median normalized length difference ranged between -0.7 and 1.7 m, and was on average equal to 0.6 m, meaning that the operators systematically overestimated the cliff area. The mean of the absolute value of the median normalized length difference was 0.8 m, which was used as an estimate for the cliff area delineation uncertainty. We conservatively assumed the same value for the Pléiades orthoimages and UAV orthomosaics, even though it should be lower for the UAV orthomosaics because of their higher resolution. For the terrestrial photogrammetry data, we assumed no uncertainty on the cliff area. The volumetric uncertainty σ_m was obtained by multiplying this value by the perimeter of cliff footprint and by the mean elevation change from DEM differences for UAV and Pléiades.

4.4.5 Accuracy of the topographic data

The uncertainty on the vertical accuracy of the terrestrial photogrammetry was directly estimated as the mean of the GCPs residual of all cliffs (0.21 m). For the UAV and Pléiades orthoimages we followed the classical assumption of partially correlated errors (Fischer et al., 2015; Rolstad et al., 2009) and therefore σ_z is given by:

$$\sigma_z = \begin{cases} A_{2D}\sigma_{\Delta h}\sqrt{\frac{A_{cor}}{5A_{2D}}} & ; A_{2D} < A_{cor} \\ A_{2D}\sigma_{\Delta h} & ; A_{2D} \geq A_{cor} \end{cases} \quad (5)$$

where $A_{cor} = \pi L^2$, with L being the decorrelation length and $\sigma_{\Delta h}$ being the normalized median of absolute difference (NMAD; Höhle and Höhle, 2009) of the elevation difference on stable ground. We experimentally determined L = 150 m for the UAV and L = 150 m for the Pléiades data, even though the spherical model was not fitting the Pléiades semi-variogram very well. We found $\sigma_{\Delta h}$ = 0.27 m for the UAV and 0.36 m for Pléiades.

The Cryosphere Discuss., https://doi.org/10.5194/tc-2018-38
Manuscript under review for journal The Cryosphere
Discussion started: 29 March 2018

Under the assumption that the different sources of uncertainty are independent, the final uncertainty on the volume estimate σ_V is:

$$\sigma_V = \sqrt{\sigma_e^2 + \sigma_d^2 + \sigma_w^2 + \sigma_m^2 + \sigma_z^2} \quad (6)$$

5 Results

5.1 Comparison of TIN based and DEM based estimates

The volume changes estimated from terrestrial photogrammetry (our reference) and from UAV / Pléiades data are in good agreement and within error bars (Table S1 and Fig. 7). The total volume loss estimated for these twelve cliffs for the period November 2015–November 2016 is 193 453 $\pm$ 19 647 m^3 a^{-1} using terrestrial photogrammetry and 188 270 $\pm$ 20 417 m^3 a^{-1} and 181 744 $\pm$ 19 436 m^3 a^{-1} using UAV and Pléiades, respectively. The total relative difference is therefore -3 % for the UAV and -7 % for Pléiades, which is smaller than the uncertainty on each estimate ($\sim$10 %, calculated as the quadratic sum of the twelve individual cliff uncertainty estimates, assumed to be independent). The total Pléiades and UAV estimates are lower than the reference estimate, nevertheless, this is probably due to the estimate of the largest cliff (cliff 01), as there is no systematic under estimation of the volume for individual cliffs (Fig. 7).

5.2 Sensitivity to the emergence velocity

As Changri Nup Glacier is a slow flowing glacier, the emergence velocity is small and the associated uncertainty is low (Fig. 6a). Nevertheless, with our dataset it is possible to explore more extreme emergence velocities up to 5 m a^{-1}, which is a value inferred for a part of the Khumbu Glacier tongue and which is also the maximum emergence velocity measured on a debris-covered tongue, to our knowledge (Nuimura et al., 2011). Our results show that, as a rule of thumb, every 1 m a^{-1} error on the emergence velocity would increase the one-year volume change estimate by 10 % (Fig. 6b). It is noteworthy that the main source of uncertainty on the cliff volume change is the uncertainty on the emergence velocity.

5.3 Importance of the glacier flow corrections

In order to check the internal consistency of the glacier flow correction, we calculated the mean glacier tongue net ablation (calculated as the mean rate of elevation change minus the emergence velocity) before and after corrections. For the period November 2015–November 2016, without flow correction the mean tongue net ablation was equal to -1.07 $\pm$ 0.27 m a^{-1} and -1.18 $\pm$ 0.36 m a^{-1} for the UAV and Pléiades DEM differences, respectively. After the glacier flow correction (Eq. 3), the mean tongue net ablation was equal to -1.10 $\pm$ 0.27 m a^{-1} and -1.20 $\pm$ 0.36 m a^{-1} for the UAV and Pléiades data, respectively. The very good consistency between each estimate gave confidence in the fact that our glacier flow correction conserves mass. The same consistency was found for the period November 2016–November 2017.

For individual cliffs, the contribution of the glacier flow corrections were small relative to the uncertainties (Fig. 7), except for cliff 11 and 12 that have a small volume contribution. These two cliffs are also located in the fastest flowing part of the

The Cryosphere Discuss., https://doi.org/10.5194/tc-2018-38
Manuscript under review for journal The Cryosphere
Discussion started: 29 March 2018

glacier tongue. The low magnitude of the glacier flow corrections is a result of (1) the small displacements of most of the cliffs and (2) the vertical displacement due to slope, which tended to compensate for the emergence velocity (Fig. 3). Nevertheless, for the two smallest and fast moving cliffs (cliffs 11 and 12), these corrections were much larger and resulted in improved estimates of volume change for both Pléiades and UAV data (Fig. 7).

5.4 Total contribution of ice cliffs to the glacier tongue net ablation for the period November 2015–November 2016

In addition to the 12 cliffs mapped in the field, we mapped 132 additional cliffs from the Pléiades and UAV orthoimages and slope maps. The total planar cliff footprint area from November 2015 and November 2016 was 113 007 $\pm$ 20 800 m^2, i.e. 7.4 % of the total tongue planar area. Averaged over this cliff mask, the UAV (respectively Pléiades) rate of elevation change corrected from glacier flow and emergence was -3.88 $\pm$ 0.27 (respectively -3.91 $\pm$ 0.36 m a^{-1}). This corresponds to a total average volume loss at ice cliffs of 439 689 $\pm$ 54 000 m^3 a^{-1}.

The three largest cliffs contribute to almost 40 % of the total net ablation from cliffs (Fig. 8). As there is some variability in the rate of cliff thinning, the volume change of each cliff is not always directly related to its area (Figs. 8 and 9). Nevertheless, the largest cliffs dominate the volume loss and all the cliffs below 2 000 m^2 contribute to less than 20 % of the total volume loss (Fig. 8).

For the same period the tongue-averaged rate of elevation change was -0.79 $\pm$ 0.21 m a^{-1} (average of the UAV and Pléiades thinning rates) which, after adding the emergence velocity, corresponds to a net glacier tongue ablation of 1.12 $\pm$ 0.21 m a^{-1} or a volume loss of 1 918 172 $\pm$ 196 431 m^3 a^{-1}. Consequently, the fraction of total net glacier tongue ablation due to cliffs was found to be 23 $\pm$ 5 % for both methods although they cover only 7.4 % of the tongue area. The factor p was thus equal to 3.1 $\pm$ 0.6.

5.5 Total contribution of ice cliffs to the glacier tongue net ablation for the period November 2016–November 2017

For the period November 2016–November 2017, we relied on the Pléiades and UAV data only. The cliff footprint area from November 2016 and November 2017 was 119 600 $\pm$ 20 800 m^2, i.e. 7.8 % of the total tongue area. Averaged over this cliff mask, the UAV (respectively Pléiades) rate of elevation change corrected for glacier flow and emergence was -4.76 $\pm$ 0.27 (respectively -4.43 $\pm$ 0.36 m a^{-1}). For the two elevation products this corresponds to an average total ice cliff volume loss of 549 943 $\pm$ 66 000 m^3 a^{-1}. In the meantime the tongue-average rate of elevation change was -1.18 $\pm$ 0.21 m a^{-1} (average of the UAV and Pléiades thinning rates), corresponding to a net glacier tongue ablation of 1.51 $\pm$ 0.21 m a^{-1} or a total volume loss of 2 308 596 $\pm$ 235 000 m^3 a^{-1}. Consequently, the ice cliffs contributed to 24 $\pm$ 5 % of the net glacier tongue ablation and the p factor was equal to 3.0 $\pm$ 0.6 for the period November 2016–November 2017.

The Cryosphere Discuss., https://doi.org/10.5194/tc-2018-38
Manuscript under review for journal The Cryosphere
Discussion started: 29 March 2018

6 Discussion

6.1 Comparison of two years of acquisition

While a comparison between only two years of data cannot be used to extrapolate our results in time, we note the similarity between the total ice cliff contribution to net ablation (23 $\pm$ 5 % and 24 $\pm$ 5 % in November 2015–November 2016 and November 2016–November 2017, respectively). In contrast, total net ablation of the Changri Nup Glacier tongue was $\sim$25 % higher for the period November 2016–November 2017 than for the period November 2015–November 2016. While a difference in meteorological conditions between these two years is a likely cause of the greater ablation totals, the ice cliffs ablate at a temporally constant rate relative to the mean tongue.

6.2 Influence of the emergence velocity and glacier flow correction on p

In most studies (Immerzeel et al., 2014; Brun et al., 2016; Thompson et al., 2016), the glacier thinning rate was assumed to be directly equal to the net ablation rate, i.e. emergence velocity was assumed to be zero. If we make the same assumption (but include the corrections for horizontal displacement and the vertical displacement due to the slope), we find a mean thinning rate of 0.80 $\pm$ 0.10 m a^{-1} for the tongue and of 3.59 $\pm$ 0.17 m a^{-1} for the cliffs (average of UAV and Pléiades data) for the period November 2015–November 2016. In this case, the factor p would be 4.5 $\pm$ 0.6, which is 50 % higher than the original value. Doing the same for the period November 2016–November 2017, the factor p would be 3.6 $\pm$ 0.6, which is 20 % higher than the original value. This might partially explain why previous studies found significantly higher values of p, and stresses the need to estimate and take into account the influence of emergence velocity, even for almost stagnant glacier tongues like Changri Nup Glacier (see Discussion below).

6.3 Ice cliff ablation and debris-cover anomaly

Between November 2011 and November 2015, Vincent et al. (2016) quantified the reduction of area-averaged net ablation over the glacier tongue due to debris-cover. They obtained a tongue-wide net ablation of -1.2 m w.e. a^{-1} and -3.0 m w.e. a^{-1} with and without debris, respectively. As ice cliffs ablate $\sim$3 times faster than the debris-covered tongue, and only $\sim$1.2 times faster than the tongue if it was entirely debris-free, 75 % of the tongue would have to be covered by ice cliffs to compensate for the lower ablation rate under debris and to achieve the same overall ablation rate as a clean ice glacier under similar conditions. As a consequence, it is unlikely that ice cliffs can explain the "debris-cover anomaly" as they typically cover a very limited area (Sakai et al., 1998; Buri et al., 2016b; Reid and Brock, 2014).

Other ablation-related processes such as supra-glacial ponds (Miles et al., 2016) or englacial hydrology (Benn et al., 2012) may contribute to higher thinning rates than what can be expected on the basis of the Østrem curve. Yet this does not apply to the case of Changri Nup Glacier, as Vincent et al. (2016) already showed that the debris part as a whole is responsible for a significant reduction of ablation on debris-covered tongues and that the insulating effect of the debris surpasses the enhanced

ablation processes. As a consequence, the reason for similar thinning rates over debris-covered and debris-free areas, i.e. the "debris-cover anomaly" can only be related to a combination of surface mass balance change and dynamics.

Indeed, let us consider theoretically one glacier with a tongue that is either debris-covered (case 1- referred hereafter as "DC") or debris-free (case 2 – referred hereafter as "DF"). In both cases, the mean glacier tongue thinning rate $\overline{\partial h/\partial t}$, follows the equation of mass conservation (Cuffey and Paterson, 2010)

$$\overline{\frac{\partial h}{\partial t}} = -\frac{1}{\rho}\dot{b} + \frac{\Phi}{A} \tag{7}$$

where Φ (m^3 a^{-1}) is the ice flux entering in the tongue of area A (m^2), ρ is the ice density (kg m^{-2}), and $\dot{b}$ is the area-averaged tongue net ablation (kg m^{-2} a^{-1}). In the upper part of this glacier above the tongue, the ice flux is similar in both cases i.e. $\Phi_{\mathrm{DC}} = \Phi_{\mathrm{DF}}$. But debris-covered glaciers have lower accumulation-area ratios than debris-free glaciers (Scherler et al., 2011). Their ablation area is thus expected to be larger ($A_{\mathrm{DC}} > A_{\mathrm{DF}}$), leading to lower emergence velocity ($w_{e,\mathrm{DC}} = \Phi/A_{\mathrm{DC}} < \Phi/A_{\mathrm{DF}} = w_{e,\mathrm{DF}}$). If the glacier is in equilibrium, in both cases, the thinning rate at any elevation is 0, because the emergence velocity compensates the surface mass balance, but with lower magnitudes for both variables in case of a debris-covered tongue (Fig. 10).

In a transient regime with consistent negative mass balances, the glacier response time of a debris covered glacier is longer compared with a debris-free glacier (Rowan et al., 2015), therefore the clean tongue will shrink faster than the debris-covered tongue, further enhancing the difference between A_{DC} and A_{DF}. The difference between emergence velocities will increase accordingly, with an enhanced emergence velocity over debris-free tongue and almost unchanged velocity over debris-covered tongue (Fig. 10). As a result and as already shown by Banerjee (2017) using a modelling approach, similar thinning rates between debris-free and debris-covered tongues are due to the fact that the combination of reduced emergence velocities and lower ablation coincidently sum up to similar thinning rates as debris-free glaciers (Fig. 10). Additionally, there are evidences of slowing down of debris-covered tongues and detachment from their accumulations area, both leading to reduction in ice flux and consequently in w_e (Neckel et al., 2017). In conclusion, this term "debris-cover anomaly" comes from a confusion between thinning rates and net ablation and in turn we recommend to abandon the term.

6.4 Automatic delineation of cliffs

Previous studies automatically digitized cliff outlines using object-based analysis workflows (Kraaijenbrink et al., 2016b), or by identifying area of large elevation change (Thompson et al., 2016). The first methodology was not applicable to Changri Nup Glacier (neither on the UAV imagery, nor on the Pléiades imagery) due to the presence of shadows and the wide range of appearances of ice cliffs on the debris-covered tongue. Lower resolution datasets would not be suitable for object-based image analysis. The automatic delineation of cliffs as areas of large elevation change may not be reliable as the elevation change distributions of cliff and off-cliff overlap (Fig. 9). A combination of these two methods (i.e. including in the elevation change component in the object-based classification) might be a promising alternative in the automatic mapping of cliff outlines.

Nevertheless, 80 % of the total cliff contribution originates from the 20 largest cliffs in our study (Fig. 8), which are less challenging to map than the smaller cliffs.

The Cryosphere Discuss., https://doi.org/10.5194/tc-2018-38
Manuscript under review for journal The Cryosphere
Discussion started: 29 March 2018

6.5 Applicability to other glaciers

Determining the total ice cliff contribution to the net ablation of the tongue, i.e. the p factor defined in this study, of a single glacier has limited value by itself, because we do not know the glacier-to-glacier variability. In particular, it is too early to conclude if the differences in the literature reflect the inconsistencies amongst the different methods used or the glacier-to-glacier variability. For instance, models (Sakai et al., 1998; Juen et al., 2014; Buri et al., 2016b; Reid and Brock, 2014) are not directly comparable with the observations (Thompson et al., 2016; Watson et al., 2017). Up to now both neglected the flow components, and we advocate for a more consistent framework. A significant obstacle to applying our method to other glaciers is the need to estimate the emergence velocity, which requires an accurate determination of the ice fluxes entering the glacier tongues. More field campaigns dedicated to ice thickness and velocity measurements (Nuimura et al., 2011, 2017) or the development of airborne ice thickness retrievals through debris are recommended.

7 Conclusions

In this study, we estimate the total contribution of ice cliff to the total net ablation of a debris-covered glacier tongue for two consecutive years, taking into account the emergence velocity. Ice cliffs are responsible for 23-24 $\pm$ 5 % of the total net ablation for both years, despite a tongue-wide net ablation approximately 25 % higher for the second year. For the case of Changri Nup Glacier, the fraction of total net ablation from ice cliffs is too low to explain by itself the so-called "debris-cover anomaly". Other contributions, such as ablation from supra-glacial lakes or englacial conduits are potentially large and have to be quantified, but for the specific case of Changri Nup Glacier they are not large enough to compensate for the reduced ablation (Vincent et al., 2016). Consequently, we hypothesize that the "debris-cover anomaly" could be a result of lower emergence velocities and reduced ablation, which leads to *thinning rates* comparable to those observed on clean ice glaciers.

Our method requires high-resolution UAV or stereo imagery, and is restricted to glaciers where thickness estimates are available and emergence velocity can be estimated. A comparison of p values calculated for other debris-covered glaciers under our suggested framework would inform estimates of ice cliff ablation for other and potentially much larger debris-covered tongues. Though our results cover only two years of data, the p value remains constant for different net ablation totals. A longer-term quantification of the relative ice-cliff contribution to net ablation is required to include these results into debris-covered glacier mass balance models.

In line with a previous study (Vincent et al., 2016), we advocate for the abandonment of the term "debris-cover anomaly", which is based on a confusion between thinning rate and net ablation, and we stress the need for more research about the emergence velocity of debris-covered tongues. Two research directions could be extensive measurements of ice thicknesses and networks of stake measurements to assess the spatial variability of the emergence.

Data availability. Data are available upon request to F.B.

Author contributions. F.B., P.W. and E.B. designed the study. F.B. and C.R. processed the terrestrial photogrammetry data. F.B. and E.B. performed the Pléiades data processing. P.K., W.I. and F.B. processed the UAV data. P.W., E.B., C.V., J.S., D.S. and F.B. collected the field data. All authors interpreted the results. F.B. led the writing of the paper and all other co-authors contributed to it.

Competing interests. The authors declare no competing interest.

Acknowledgements. This work has been supported by the French Service d'Observation GLACIOCLIM, the French National Research Agency (ANR) through ANR-13-SENV-0005-04-PRESHINE, and has been supported by a grant from Labex OSUG@2020 (Investissements d'avenir – ANR10 LABX56). This study was carried out within the framework of the Ev-K2-CNR Project in collaboration with the Nepal Academy of Science and Technology as foreseen by the Memorandum of Understanding between Nepal and Italy, and thanks to contributions from the Italian National Research Council, the Italian Ministry of Education, University and Research and the Italian Ministry of Foreign Affairs. Funding for the UAV survey was generously provided by the United Kingdom Department for International Development (DFID) and by the Ministry of Foreign Affairs, Government of Norway. This project has received funding from the European Research Council (ERC) under the European Union's Horizon 2020 research and innovation programme (grant agreement No 676819). E.B. acknowledges support from the French Space Agency (CNES) and the Programme National de Télédétection Spatiale grant PNTS-2016-01. The International Centre for Integrated Mountain Development is funded in part by the governments of Afghanistan, Bangladesh, Bhutan, China, India, Myanmar, Nepal, and Pakistan. The views expressed are those of the authors and do not necessarily reflect their organizations or funding institutions. F.B., P.W., C.V. and Y.A are parts of Labex OSUG@2020 (ANR10 LABX56).

References

Agarwal, V., Bolch, T., Syed, T. H., Pieczonka, T., Strozzi, T., and Nagaich, R.: Area and mass changes of Siachen Glacier (East Karakoram), Journal of Glaciology, 63, 148–163, https://doi.org/10.1017/jog.2016.127, 2017.

Agisoft, L.: Agisoft PhotoScan User Manual: Professional Edition, Version 1.3, 2017.

Anderson, L. S. and Anderson, R. S.: Modeling debris-covered glaciers: response to steady debris deposition, The Cryosphere, 10, 1105–1124, https://doi.org/10.5194/tc-10-1105-2016, https://www.the-cryosphere.net/10/1105/2016/, 2016.

Banerjee, A.: Brief communication: Thinning of debris-covered and debris-free glaciers in a warming climate, The Cryosphere, 11, 133–138, https://doi.org/10.5194/tc-11-133-2017, https://www.the-cryosphere.net/11/133/2017/, 2017.

Belart, J. M. C., Berthier, E., Magnússon, E., Anderson, L. S., Pálsson, F., Thorsteinsson, T., Howat, I. M., Aðalgeirsdóttir, G., Jóhannesson, T., and Jarosch, A. H.: Winter mass balance of Drangajökull ice cap (NW Iceland) derived from satellite sub-meter stereo images, The Cryosphere, 11, 1501–1517, https://doi.org/10.5194/tc-11-1501-2017, https://www.the-cryosphere.net/11/1501/2017/, 2017.

Benn, D., Bolch, T., Hands, K., Gulley, J., Luckman, A., Nicholson, L., Quincey, D., Thompson, S., Toumi, R., and Wiseman, S.: Response of debris-covered glaciers in the Mount Everest region to recent warming, and implications for outburst flood hazards, Earth-Science Reviews, 114, 156–174, https://doi.org/10.1016/j.earscirev.2012.03.008, 2012.

Berthier, E., Arnaud, Y., Kumar, R., Ahmad, S., Wagnon, P., and Chevallier, P.: Remote sensing estimates of glacier mass balances in the Himachal Pradesh (Western Himalaya, India), Remote Sensing of Environment, 108, 327–338, https://doi.org/10.1016/j.rse.2006.11.017, 2007.

Brun, F., Buri, P., Miles, E. S., Wagnon, P., Steiner, J. F., Berthier, E., Ragettli, S., Kraaijenbrink, P., Immerzeel, W., and Pellicciotti, F.: Quantifying volume loss from ice cliffs on debris-covered glaciers using high-resolution terrestrial and aerial photogrammetry, Journal of Glaciology, 62, 684–695, https://doi.org/10.1017/jog.2016.54, http://journals.cambridge.org.gaelnomade.ujf-grenoble.fr/article_S002214301600054X, 2016.

Buri, P., Miles, E. S., Steiner, J. F., Immerzeel, W. W., Wagnon, P., and Pellicciotti, F.: A physically based 3-D model of ice cliff evolution over debris-covered glaciers, Journal of Geophysical Research: Earth Surface, 121, 2471–2493, https://doi.org/10.1002/2016JF004039, https://doi.org/10.1002/2016JF004039, 2016a.

Buri, P., Pellicciotti, F., Steiner, J. F., Miles, E. S., and Immerzeel, W. W.: A grid-based model of backwasting of supraglacial ice cliffs on debris-covered glaciers, Annals of Glaciology, 57, 199–211, https://doi.org/10.3189/2016aog71a059, http://dx.doi.org/10.3189/2016AoG71A059, 2016b.

Cuffey, K. M. and Paterson, W. S. B.: The physics of glaciers, Academic Press, 2010.

Fischer, M., Huss, M., and Hoelzle, M.: Surface elevation and mass changes of all Swiss glaciers 1980–2010, The Cryosphere, 9, 525–540, https://doi.org/10.5194/tc-9-525-2015, http://www.the-cryosphere.net/9/525/2015/, 2015.

Gardelle, J., Berthier, E., Arnaud, Y., and Kääb, A.: Region-wide glacier mass balances over the Pamir-Karakoram-Himalaya during 1999-2011, The Cryosphere, 7, 1263–1286, https://doi.org/10.5194/tc-7-1263-2013, 2013.

Gindraux, S., Boesch, R., and Farinotti, D.: Accuracy Assessment of Digital Surface Models from Unmanned Aerial Vehicles' Imagery on Glaciers, Remote Sensing, 9, https://doi.org/10.3390/rs9020186, http://www.mdpi.com/2072-4292/9/2/186, 2017.

Höhle, J. and Höhle, M.: Accuracy assessment of digital elevation models by means of robust statistical methods, {ISPRS} Journal of Photogrammetry and Remote Sensing, 64, 398 – 406, https://doi.org/http://dx.doi.org/10.1016/j.isprsjprs.2009.02.003, http://www.sciencedirect.com/science/article/pii/S0924271609000276, 2009.

Hooke, R. L.: Principles of glacier mechanics, Cambridge university press, 2005.

Immerzeel, W., Kraaijenbrink, P., Shea, J., Shrestha, A., Pellicciotti, F., Bierkens, M., and de Jong, S.: High-resolution monitoring of Himalayan glacier dynamics using unmanned aerial vehicles, Remote Sensing of Environment, 150, 93–103, https://doi.org/10.1016/j.rse.2014.04.025, 2014.

Juen, M., Mayer, C., Lambrecht, A., Han, H., and Liu, S.: Impact of varying debris cover thickness on ablation: a case study for Koxkar Glacier in the Tien Shan, The Cryosphere, 8, 377–386, https://doi.org/10.5194/tc-8-377-2014, http://www.the-cryosphere.net/8/377/2014/, 2014.

Kääb, A., Berthier, E., Nuth, C., Gardelle, J., and Arnaud, Y.: Contrasting patterns of early twenty-first-century glacier mass change in the Himalayas, Nature, 488, 495–498, https://doi.org/10.1038/nature11324, 2012.

Kraaijenbrink, P., Meijer, S. W., Shea, J. M., Pellicciotti, F., Jong, S. M. D., and Immerzeel, W. W.: Seasonal surface velocities of a Himalayan glacier derived by automated correlation of unmanned aerial vehicle imagery, Annals of Glaciology, 57, 103–113, https://doi.org/10.3189/2016aog71a072, http://dx.doi.org/10.3189/2016AoG71A072, 2016a.

Kraaijenbrink, P. D. A., Shea, J. M., Pellicciotti, F., Jong, S. M. d., and Immerzeel, W. W.: Object-based analysis of unmanned aerial vehicle imagery to map and characterise surface features on a debris-covered glacier, Remote Sensing of Environment, 186, 581 – 595, https://doi.org/https://doi.org/10.1016/j.rse.2016.09.013, http://www.sciencedirect.com/science/article/pii/S003442571630356X, 2016b.

Kraaijenbrink, P. D. A., Bierkens, M. F. P., Lutz, A. F., and Immerzeel, W. W.: Impact of a global temperature rise of 1.5 degrees Celsius on Asia glaciers, Nature, 549, 257–260, https://doi.org/10.1038/nature23878, 2017.

Lamsal, D., Fujita, K., and Sakai, A.: Surface lowering of the debris-covered area of Kanchenjunga Glacier in the eastern Nepal Himalaya since 1975, as revealed by Hexagon KH-9 and ALOS satellite observations, The Cryosphere, 11, 2815–2827, https://doi.org/10.5194/tc-11-2815-2017, https://www.the-cryosphere.net/11/2815/2017/, 2017.

Lejeune, Y., Bertrand, J.-M., Wagnon, P., and Morin, S.: A physically based model of the year-round surface energy and mass balance of debris-covered glaciers, Journal of Glaciology, 59, 327–344, https://doi.org/10.3189/2013JoG12J149, 2013.

Leprince, S., Ayoub, F., Klingert, Y., and Avouac, J.-P.: Co-Registration of Optically Sensed Images and Correlation (COSI-Corr): an operational methodology for ground deformation measurements, in: Geoscience and Remote Sensing Symposium, 2007. IGARSS 2007. IEEE International, pp. 1943–1946, https://doi.org/10.1109/IGARSS.2007.4423207, 2007.

Marti, R., Gascoin, S., Berthier, E., de Pinel, M., Houet, T., and Laffly, D.: Mapping snow depth in open alpine terrain from stereo satellite imagery, The Cryosphere, 10, 1361–1380, https://doi.org/10.5194/tc-10-1361-2016, https://www.the-cryosphere.net/10/1361/2016/, 2016.

Miles, E. S., Pellicciotti, F., Willis, I. C., Steiner, J. F., Buri, P., and Arnold, N. S.: Refined energy-balance modelling of a supraglacial pond, Langtang Khola, Nepal, Annals of Glaciology, 57, 29–40, https://doi.org/10.3189/2016AoG71A421, 2016.

Neckel, N., Loibl, D., and Rankl, M.: Recent slowdown and thinning of debris-covered glaciers in south-eastern Tibet, Earth and Planetary Science Letters, 464, 95–102, https://doi.org/10.1016/j.epsl.2017.02.008, 2017.

Nicholson, L. and Benn, D. I.: Calculating ice melt beneath a debris layer using meteorological data, Journal of Glaciology, 52, 463–470, https://doi.org/10.3189/172756506781828584, 2006.

Nuimura, T., Fujita, K., Fukui, K., Asahi, K., Aryal, R., and Ageta, Y.: Temporal Changes in Elevation of the Debris-Covered Ablation Area of Khumbu Glacier in the Nepal Himalaya since 1978, Arctic, Antarctic, and Alpine Research, 43, 246–255, https://doi.org/10.1657/1938-4246-43.2.246, http://www.aaarjournal.org/doi/abs/10.1657/1938-4246-43.2.246, 2011.

Nuimura, T., Fujita, K., Yamaguchi, S., and Sharma, R. R.: Elevation changes of glaciers revealed by multitemporal digital elevation models calibrated by GPS survey in the Khumbu region, Nepal Himalaya, 1992-2008, Journal of Glaciology, 58, 648–656, https://doi.org/10.3189/2012JoG11J061, 2012.

Nuimura, T., Fujita, K., and Sakai, A.: Downwasting of the debris-covered area of Lirung Glacier in Langtang Valley, Nepal Himalaya, from 1974 to 2010, Quaternary International, https://doi.org/http://dx.doi.org/10.1016/j.quaint.2017.06.066, http://www.sciencedirect.com/science/article/pii/S1040618216313295, 2017.

Nuth, C. and Kääb, A.: Co-registration and bias corrections of satellite elevation data sets for quantifying glacier thickness change, The Cryosphere, 5, 271–290, https://doi.org/10.5194/tc-5-271-2011, http://www.the-cryosphere.net/5/271/2011/, 2011.

Pellicciotti, F., Stephan, C., Miles, E., Herreid, S., Immerzeel, W. W., and Bolch, T.: Mass-balance changes of the debris-covered glaciers in the Langtang Himal, Nepal, from 1974 to 1999, Journal of Glaciology, 61, 373–386, https://doi.org/10.3189/2015jog13j237, 2015.

Pfeffer, W. T., Arendt, A. A., Bliss, A., Bolch, T., Cogley, J. G., Gardner, A. S., Hagen, J.-O., Hock, R., Kaser, G., Kienholz, C., Miles, E. S., Moholdt, G., Mölg, N., Paul, F., Radic, V., Rastner, P., Raup, B. H., Rich, J., and Sharp, M. J.: The Randolph Glacier Inventory: a globally complete inventory of glaciers, Journal of Glaciology, 60, 537–552, https://doi.org/10.3189/2014JoG13J176, 2014.

Reid, T. and Brock, B.: Assessing ice-cliff backwasting and its contribution to total ablation of debris-covered Miage glacier, Mont Blanc massif, Italy, Journal of Glaciology, 60, 3–13, https://doi.org/10.3189/2014JoG13J045, http://www.ingentaconnect.com/content/igsoc/jog/2014/00000060/00000219/art00001, 2014.

Reid, T. D. and Brock, B. W.: An energy-balance model for debris-covered glaciers including heat conduction through the debris layer, Journal of Glaciology, 56, 903–916, https://doi.org/10.3189/002214310794457218, 2010.

Reznichenko, N., Davies, T., Shulmeister, J., and McSaveney, M.: Effects of debris on ice-surface melting rates: an experimental study, Journal of Glaciology, 56, 384–394, https://doi.org/10.3189/002214310792447725, 2010.

Rolstad, C., Haug, T., and Denby, B.: Spatially integrated geodetic glacier mass balance and its uncertainty based on geostatistical analysis: application to the western Svartisen ice cap, Norway, Journal of Glaciology, 55, 666–680, https://doi.org/10.3189/002214309789470950, 2009.

Rowan, A. V., Egholm, D. L., Quincey, D. J., and Glasser, N. F.: Modelling the feedbacks between mass balance, ice flow and debris transport to predict the response to climate change of debris-covered glaciers in the Himalaya, Earth and Planetary Science Letters, 430, 427–438, https://doi.org/10.1016/j.epsl.2015.09.004, 2015.

Sakai, A., Nakawo, M., and Fujita, K.: Melt rate of ice cliffs on the Lirung Glacier, Nepal Himalayas, 1996, Bulletin of Glacier Research, 16, 57–66, http://ci.nii.ac.jp/naid/10002475281/en, 1998.

Sakai, A., Nakawo, M., and Fujita, K.: Distribution characteristics and energy balance of ice cliffs on debris-covered glaciers, Nepal Himalaya, Arctic, Antarctic and Alpine Research, 34, 12–19, 2002.

Scherler, D., Bookhagen, B., and Strecker, M. R.: Hillslope-glacier coupling: The interplay of topography and glacial dynamics in High Asia, Journal of Geophysical Research: Earth Surface, 116, https://doi.org/10.1029/2010JF001751, http://dx.doi.org/10.1029/2010JF001751, 2011.

Shean, D. E., Alexandrov, O., Moratto, Z. M., Smith, B. E., Joughin, I. R., Porter, C., and Morin, P.: An automated, open-source pipeline for mass production of digital elevation models (DEMs) from very-high-resolution commercial stereo satellite imagery, {ISPRS} Journal of Photogrammetry and Remote Sensing, 116, 101 – 117, https://doi.org/http://dx.doi.org/10.1016/j.isprsjprs.2016.03.012, http://www.sciencedirect.com/science/article/pii/S0924271616300107, 2016.

Sherpa, S. F., Wagnon, P., Brun, F., Berthier, E., Vincent, C., Lejeune, Y., Arnaud, Y., Kayastha, R. B., and Sinisalo, A.: Contrasted surface mass balances of debris-free glaciers observed between the southern and the inner parts of the Everest region (2007-2015), Journal of Glaciology, 63, 637–651, 2017.

Steiner, J. F., Pellicciotti, F., Buri, P., Miles, E. S., Immerzeel, W. W., and Reid, T. D.: Modelling ice-cliff backwasting on a debris-covered glacier in the Nepalese Himalaya, Journal of Glaciology, 61, 889–907, https://doi.org/10.3189/2015jog14j194, http://dx.doi.org/10.3189/2015JoG14J194, 2015.

Østrem, G.: Ice Melting under a Thin Layer of Moraine, and the Existence of Ice Cores in Moraine Ridges, Geografiska Annaler, 41, pp. 228–230, http://www.jstor.org/stable/4626805, 1959.

Thompson, S., Benn, D. I., Mertes, J., and Luckman, A.: Stagnation and mass loss on a Himalayan debris-covered glacier: processes, patterns and rates, Journal of Glaciology, 62, 467–485, https://doi.org/10.1017/jog.2016.37, 2016.

Vincent, C., Wagnon, P., Shea, J. M., Immerzeel, W. W., Kraaijenbrink, P., Shrestha, D., Soruco, A., Arnaud, Y., Brun, F., Berthier, E., and Sherpa, S. F.: Reduced melt on debris-covered glaciers: investigations from Changri Nup Glacier, Nepal, The Cryosphere, 10, 1845–1858, https://doi.org/10.5194/tc-10-1845-2016, http://www.the-cryosphere.net/10/1845/2016/, 2016.

Watson, C. S., Quincey, D. J., Smith, M. W., Carrivick, J. L., Rowan, A. V., and James, M. R.: Quantifying ice cliff evolution with multi-temporal point clouds on the debris-covered Khumbu Glacier, Nepal, Journal of Glaciology, 63, 823–837, 2017.

Wu, K., Liu, S., Jiang, Z., Xu, J., Wei, J., and Guo, W.: Recent glacier mass balance and area changes in the Kangri Karpo Mountains from DEMs and glacier inventories, The Cryosphere, 12, 103–121, https://doi.org/10.5194/tc-12-103-2018, https://www.the-cryosphere.net/12/103/2018/, 2018.

The Cryosphere Discuss., https://doi.org/10.5194/tc-2018-38
Manuscript under review for journal The Cryosphere
Discussion started: 29 March 2018

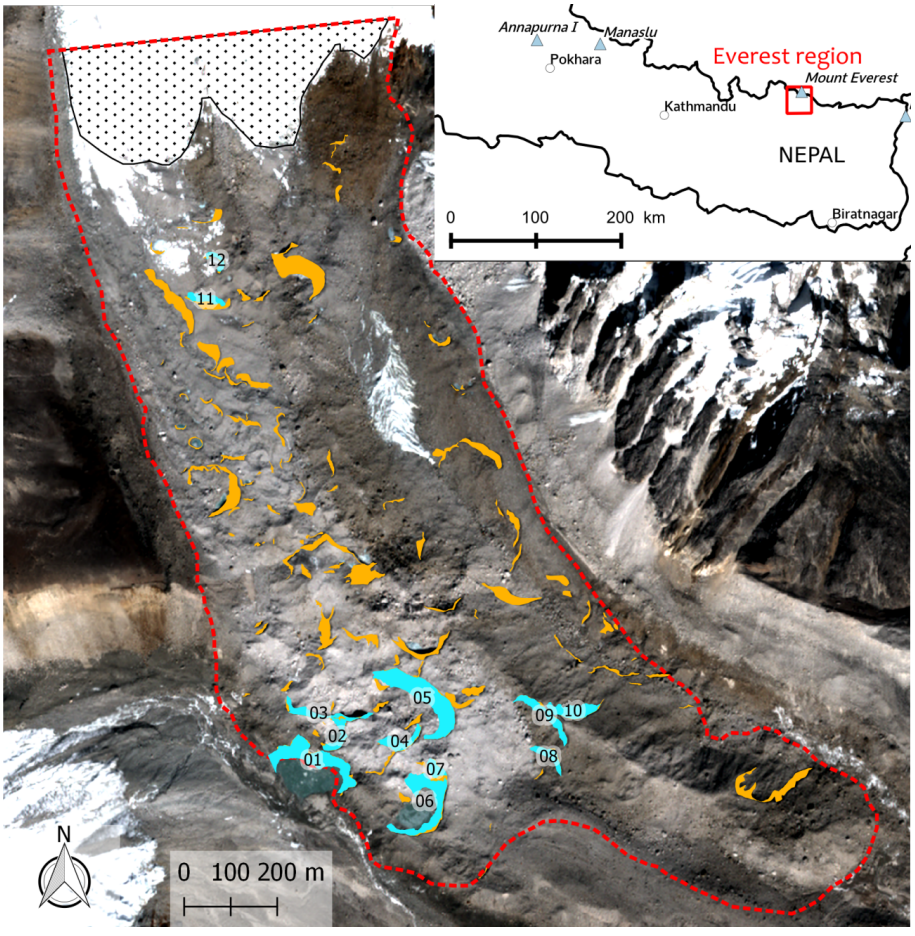

Figure 1. Map of Changri Nup Glacier tongue (red outline). The light blue shapes are the twelve cliffs surveyed with the terrestrial photogrammetry and the orange shapes are all the cliffs of the tongue. The background image is the Pléiades images of November 2016 (copyright: CNES 2016, Distribution Airbus D&S). The ice thickness was measured along the upper line of the glacier tongue outline in 2011 (Vincent et al., 2016). The dotted area is the debris-free part of the tongue (measured on November 2017).

The Cryosphere Discuss., https://doi.org/10.5194/tc-2018-38
Manuscript under review for journal The Cryosphere
Discussion started: 29 March 2018

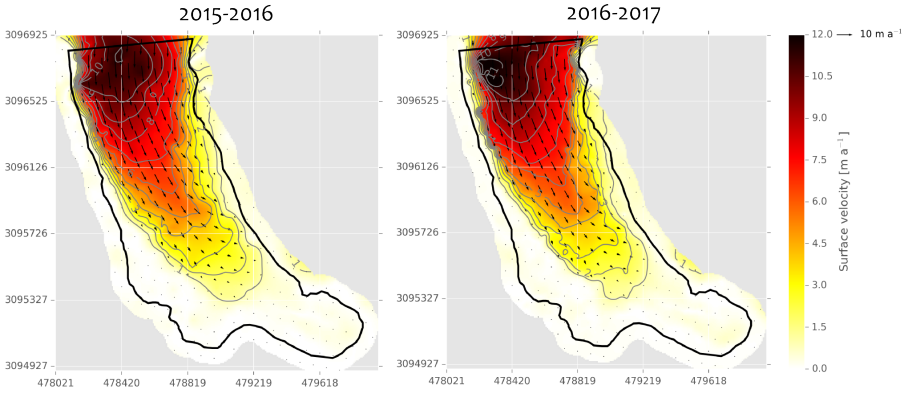

Figure 2. Annual horizontal velocity fields deduced from the correlation of Pléiades orthoimages. The field is linearly interpolated in the area of missing data.

The Cryosphere Discuss., https://doi.org/10.5194/tc-2018-38
Manuscript under review for journal The Cryosphere
Discussion started: 29 March 2018

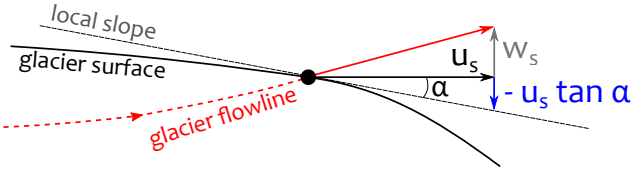

Figure 3. Definition of the different flow components, adapted from Hooke (2005).

The Cryosphere Discuss., https://doi.org/10.5194/tc-2018-38
Manuscript under review for journal The Cryosphere
Discussion started: 29 March 2018

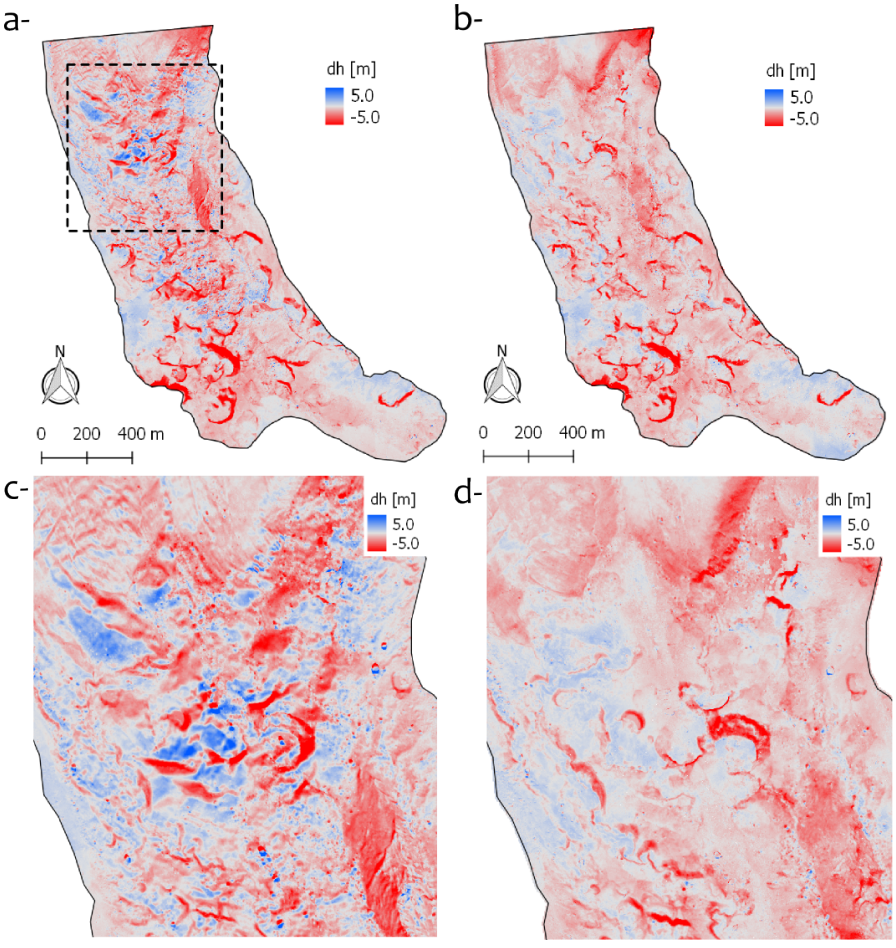

Figure 4. Panels showing maps of: raw elevation change for UAV (a, c), elevation change corrected from flow for UAV (b, d). The panels c and d correspond to a zoom in the dashed rectangle (a).

The Cryosphere Discuss., https://doi.org/10.5194/tc-2018-38
Manuscript under review for journal The Cryosphere
Discussion started: 29 March 2018

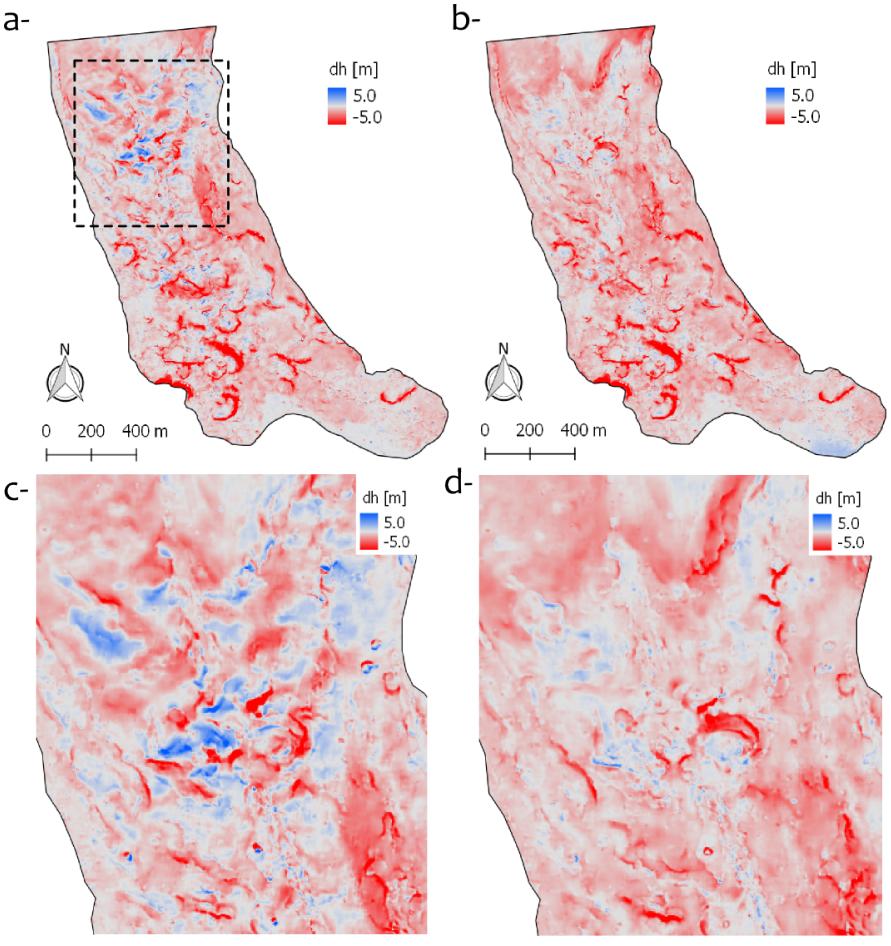

Figure 5. Panels showing maps of: raw elevation change for Pléiades (a, c), elevation change corrected from flow for Pléiades (b, d). The panels c and d correspond to a zoom in the dashed rectangle (a).

The Cryosphere Discuss., https://doi.org/10.5194/tc-2018-38
Manuscript under review for journal The Cryosphere
Discussion started: 29 March 2018

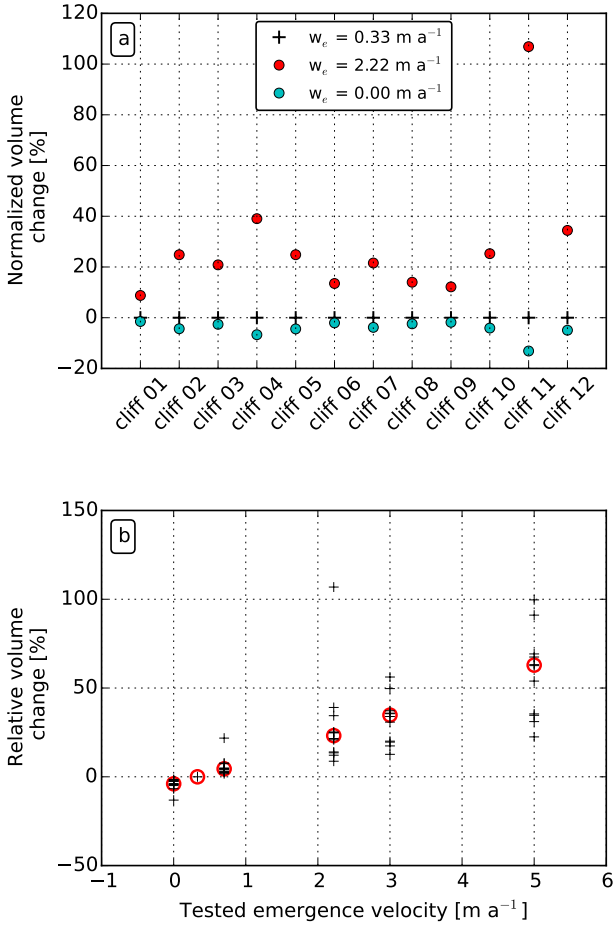

Figure 6. Sensitivity of the normalized volume change estimate to the emergence velocity for each cliff with two tested emergence velocities (a) and for all cliffs with various emergence velocities tested (b). In the latter, each cross represent a cliff and the open circles represent the median, note that cliff 11 relative volume change is not visible for emergence velocities higher than 2.2 m a^{-1}, because it is more than 150 %. The volume estimates are from terrestrial photogrammetry data.

The Cryosphere Discuss., https://doi.org/10.5194/tc-2018-38
Manuscript under review for journal The Cryosphere
Discussion started: 29 March 2018

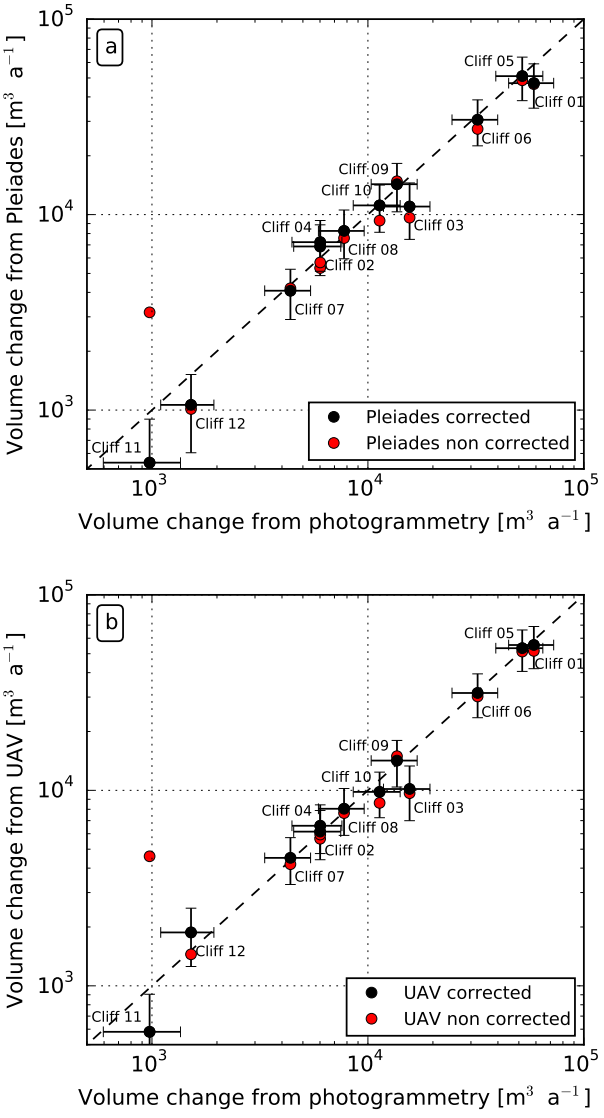

Figure 7. Comparison of the ice cliff volume changes estimated from DEM differences between UAV (a) or Pléiades (b) and terrestrial photogrammetry. Note the log scale. For each panel, "corrected" means taking into account the geometric corrections due to glacier flow and "non corrected" means neglecting them.

The Cryosphere Discuss., https://doi.org/10.5194/tc-2018-38
Manuscript under review for journal The Cryosphere
Discussion started: 29 March 2018

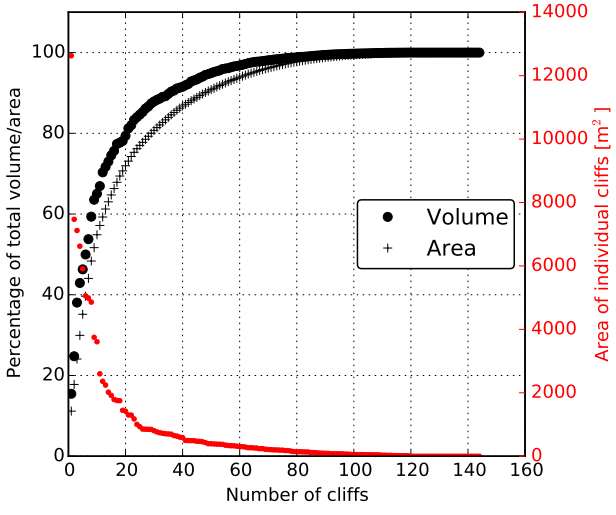

Figure 8. Individual ice cliff contributions for the period November 2015–November 2016 based on the UAV data. The left axis shows the cumulative volume (black dots) and area (black crosses), expressed as a percentage of the total volume or area, respectively.

The Cryosphere Discuss., https://doi.org/10.5194/tc-2018-38
Manuscript under review for journal The Cryosphere
Discussion started: 29 March 2018

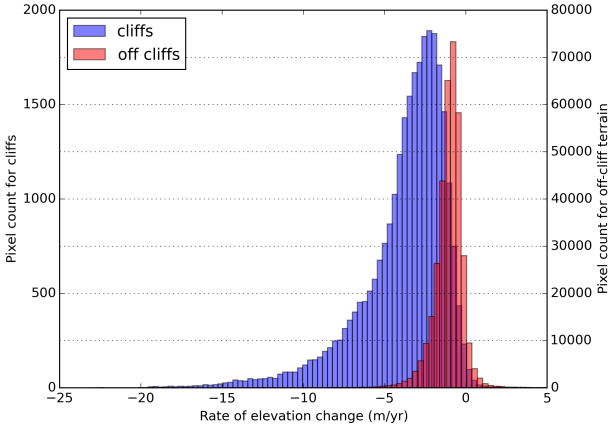

Figure 9. Rate of glacier surface elevation change for cliff and off-cliff terrain (Pléiades DEM difference November 2015–November 2016, corrected from flow). Note the strongly different Y axis.

The Cryosphere Discuss., https://doi.org/10.5194/tc-2018-38
Manuscript under review for journal The Cryosphere
Discussion started: 29 March 2018

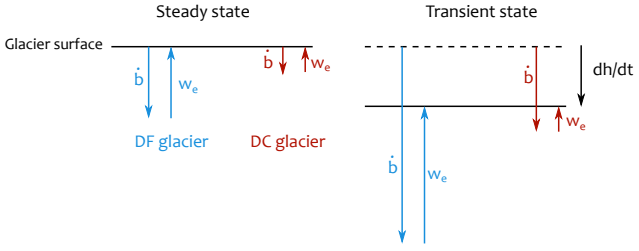

Figure 10. Conceptual representation of the interplay of net ablation ($\dot{b}$) and emergence velocity (w_e) for debris-free (DF, blue color) and debris-covered (DC, brown color) glacier tongues. In the left panel both glaciers are at equilibrium (no thinning) and in the right panel their tongues are thinning at the same rate $\overline{\partial h/\partial t}$. In the transient state, the ratio between the net ablation of debris-free tongue, the net ablation of debris-covered tongue and the emergence velocity of the debris-covered tongue is based on Vincent et al. (2016). For the steady state, we assumed a similar ratio of net ablation for debris-free and debris-covered tongues and similar emergence velocity for the debris-covered tongue, we deduced the emergence velocity of the debris-free tongue accordingly.

The Cryosphere Discuss., https://doi.org/10.5194/tc-2018-38
Manuscript under review for journal The Cryosphere
Discussion started: 29 March 2018

Table 1. Characteristics of the 12 surveyed cliffs. The 3D mean area (A_{3D}) was calculated as the mean of the November 2015 and 2016 areas, which were measured from the PCs obtained with the terrestrial photogrammetry on CloudCompare. The perimeter calculated from the cliff footprint of November 2015 and 2016. The main aspects were calculated by fitting a plan through the cliff PC or through parts of the PC in CloudCompare, the main aspect is in bold when it was possible to determine it.

Cliff ID	3D mean area [m^2]	Cliff footprint [m^2]	Footprint perimeter [m]	Main aspects (slope)
Cliff 01	7543	6575	711	**SW** (44°) / S (46°) / W (39°) / NE (59°)
Cliff 02	1315	1406	260	SW (25°) / NW (29°)
Cliff 03	3033	1821	479	**N** (69°)
Cliff 04	1851	1774	286	**N** (42°) / NW (57°) / E (36°)
Cliff 05	11294	8592	607	**SW** (44°) / NW (51°)
Cliff 06	5267	5064	639	N (60°) / W (52°) / S (45°) / SW (86°)
Cliff 07	752	979	153	**SW** (41°)
Cliff 08	1282	1307	227	S (58°) / SW (59°)
Cliff 09	2408	2263	386	**SW** (60°) / S (46°)
Cliff 10	2426	2521	284	**N** (35°)
Cliff 11	775	630	194	**N** (38°)
Cliff 12	587	653	165	W (58°) / SW (50°) / S (40°)

The Cryosphere Discuss., https://doi.org/10.5194/tc-2018-38
Manuscript under review for journal The Cryosphere
Discussion started: 29 March 2018

Table 2. Characteristics of the three UAV flights. The horizontal and vertical residuals are assessed on independent additional GCPs (Agisoft, 2017).

Date of acquisition	Number of images	Number of GCPs	Number of virtual GCPs	Horizontal residuals (cm)	Vertical residuals (cm)
22–24/11/2015	582	24	0	4	10
16/11/2016	475	17	16	N/A	N/A
23/11/2017	390	30	0	11	14

The Cryosphere Discuss., https://doi.org/10.5194/tc-2018-38
Manuscript under review for journal The Cryosphere
Discussion started: 29 March 2018

Table 3. Characteristics and IDs of the Pléiades images. Horizontal shifts relative to the UAV ortho-images are also given.

Date of acquisition	B/H	Shift eastward (m)	Shift northward (m)
22/11/2015	0.36;0.26;0.10	-4.3	0.3
13/11/2016	0.47;0.28; 0.20	6.6	3.7
24/10/2017	0.34;0.25;0.09	1.0	4.2